



**PARAMount**

*imProved Accessibility: Reliability and security  
of Alpine transport infrastructure  
related to mountainous hazards in a changing climate*

## **DEFENSE**

### **(DEbris Flows triggERed by storms - Nowcasting SystEm)**

version: 1 (Act. 6.4 - output results)

date: April 2012

author: PP7

(corresponding to [davide.tiranti@arpa.piemonte.it](mailto:davide.tiranti@arpa.piemonte.it))



*PARAMount is supported by means of the European Regional Development Fund (ERDF)*



---

## Table of contents

1	Introduction .....	1
2	Debris flows forecasting approach .....	4
3	The Radar Storm Tracking.....	5
4	The DEFENSE (DEbris Flows triggERed by storms - Nowcasting SystEm) model.....	8
5	DEFENSE operational results in Susa Valley.....	11
6	Concluding remarks .....	16
	Acknowledgements .....	16
	References .....	16
	Table of figures .....	17

# 1 Introduction

Most of the processes occurring in alpine catchments are linked to the human activities developed in fan areas. Several studies on hazard and risk analyses associated with these processes were carried out in the last decades. In this study a new multidisciplinary approach able to characterise debris flows (DF), their causes and triggering, is proposed according to previous preliminary researches. A new basins classification methodology based on proposal by Tiranti et al. (2008) suggests that hazard evaluation in mountainous areas depends on proper identification of the basins characteristics (main catchment lithology, dominant sedimentary processes, torrential processes frequency, triggering seasonality and rainfall type). This preliminary study was focused on 12 basins located in different lithological environments in the Central-Western Italian Alps. The research was then tested and refined in all the Western Italian Alps, where a great variability in terms of geomorphology, geological units and climate contexts is given. All the Susa Valley (Western Italian Alps) basins were classified from a geological, sedimentological, geomorphological, climate and historical point of view, in order to identify their features and classify them for a torrential processes hazard evaluation in all the Piemonte region. The resulting of regional application of this geological model confirms the three basin classes identified in the upper part of Susa Valley (Fig. 1); each catchment class is characterized by different bedrock lithology, basin area/fan area ratio, alluvial fan architecture, depositional style and triggering rainfall intensity, according to Tiranti (2008).

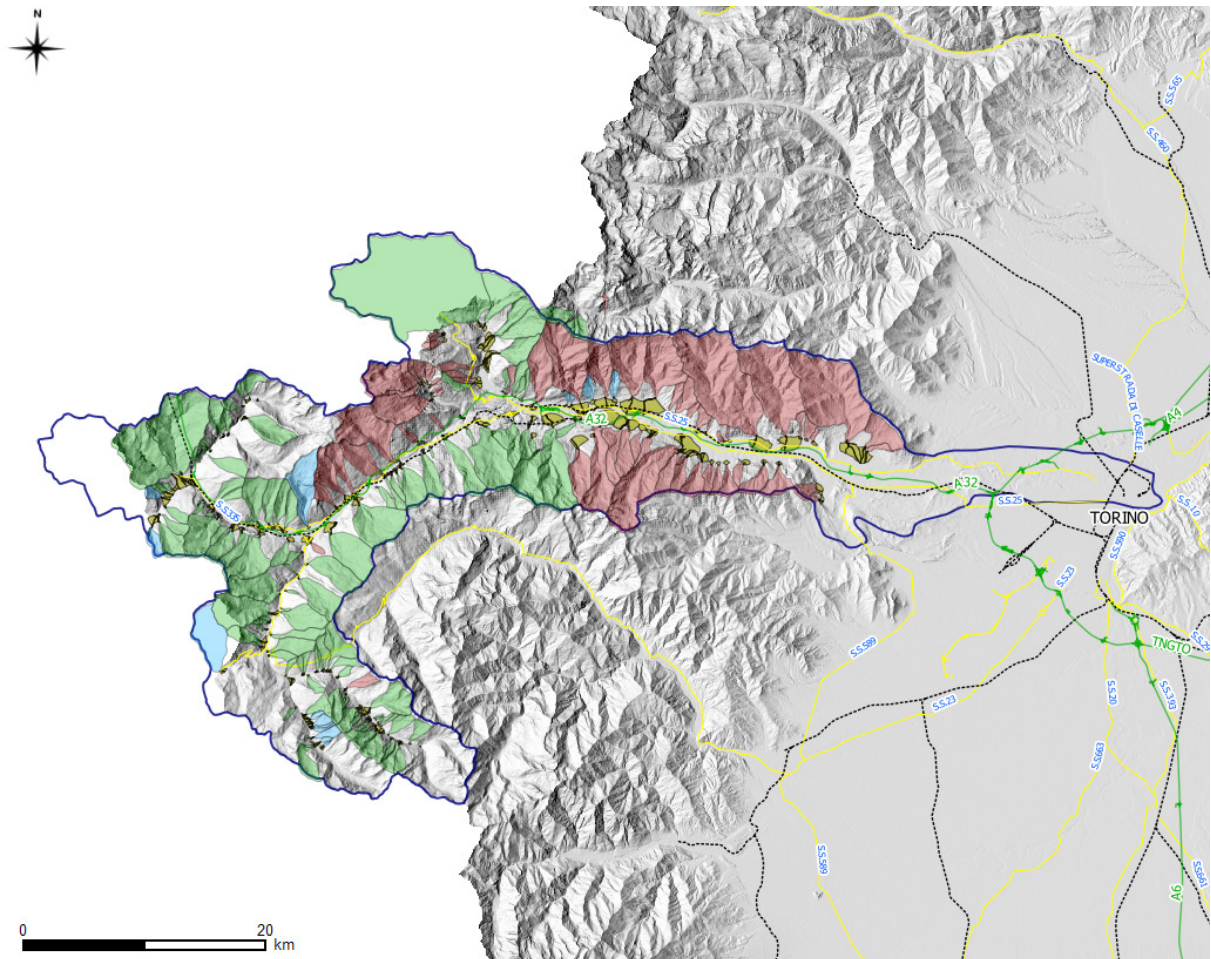


**Figure 1 :** The classified basins of Susa Valley: G1 basins in light blue; G2 basins in green; G3 basins in dark red.

Moreover, the nature of the processes that occur in a basin also depends on morphometric characteristics of the basin. In fact, thought a new index based on Melton index, the average gradient

and length of the main channel, it is possible to identify the most likely type of process can occur in a basin: flash flood, debris flood or debris flow (based on Wilford et al. 2004):

- Flash Flood (FF): flow with low sediment concentrations (< 20%);
- Debris flood (DFd): flow with even high sediment concentrations (< 50%);
- Debris flow (DFw): flow with very high sediment concentration (>50%), where the solid component prevails over the liquid one.

The basins of Susa Valley was also classified by main expected phenomenon, as shown in graph of figure 2 and in figure 3.

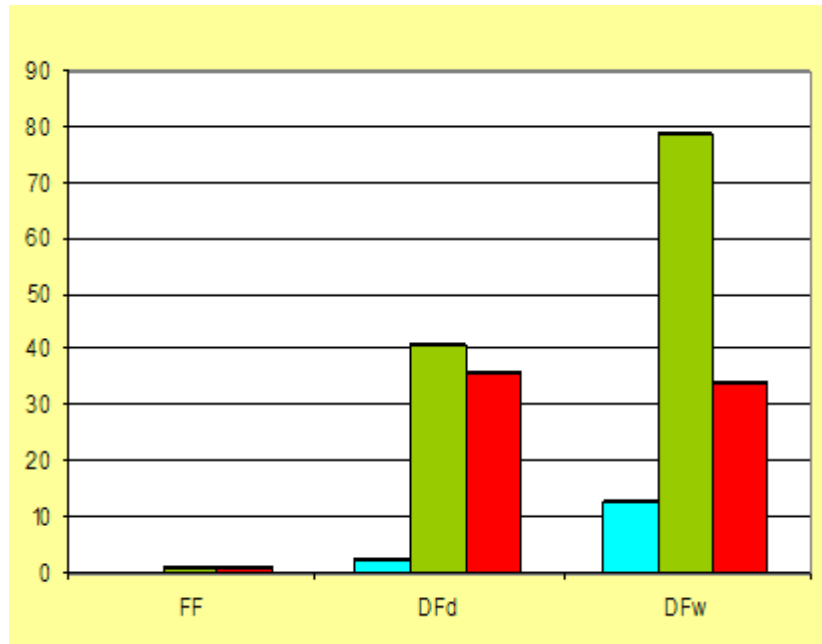


**Figure 2:** The graph represents the basins of Susa Valley subdivided by lithological group and statistical occurrence of process types in each group. G1 in light-blue, G2 in green, G3 in red; FF = flash flood; DFd = debris flood; DFw = debris flow.

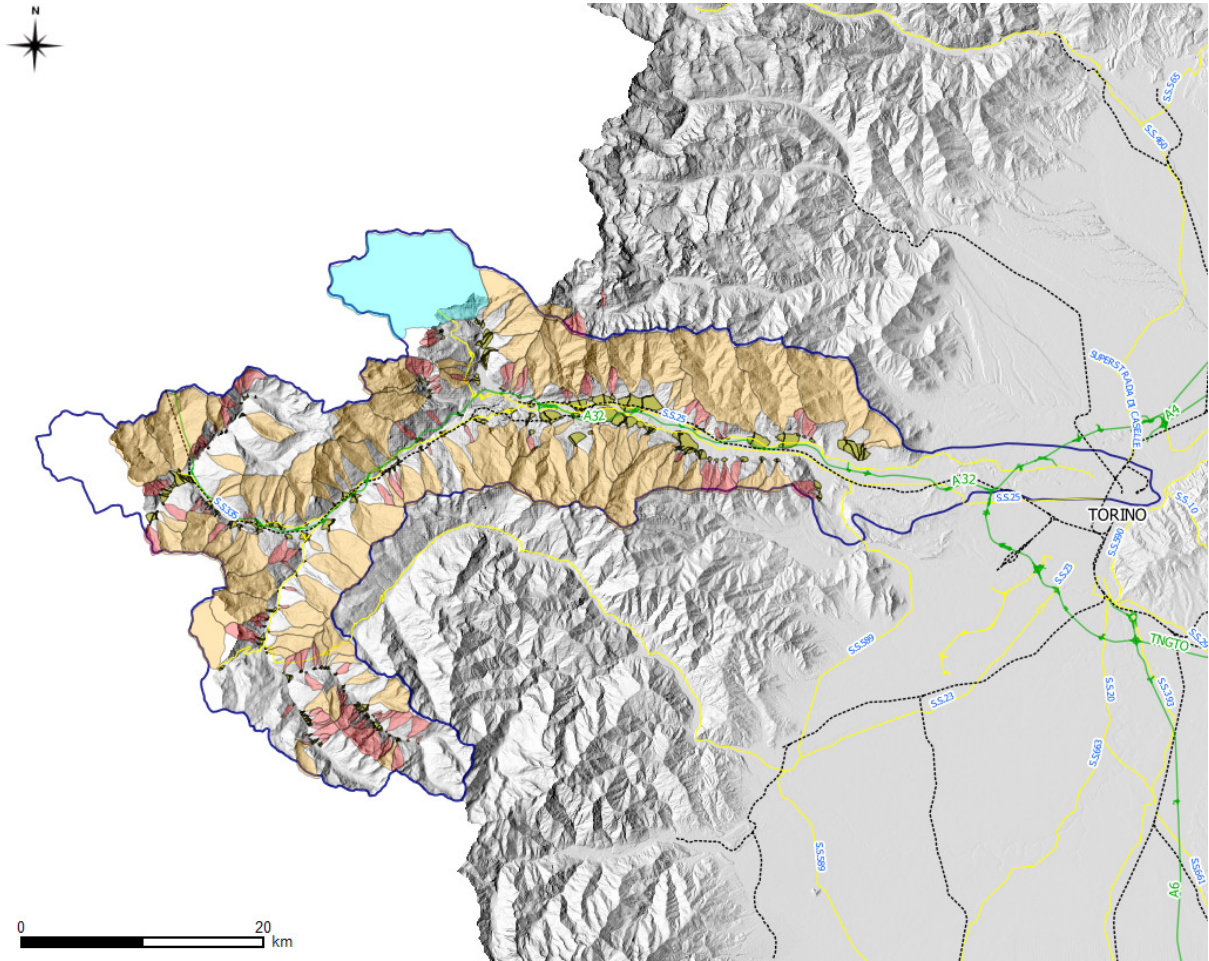


**Figure 3:** Main expected phenomena in Susa Valley's basins. Flash Flood in light blue; Debris Flood in orange; Debris Flow in red.

## 2 Debris flows forecasting approach

Traditional warning systems are usually based on rainfall rate thresholds derived by rain gauges, but rain gauges networks are often inadequate to properly identify localized storms (Duncan, 1973). Polarimetric C-band radar can provide reliable real-time rainfall estimation with high spatial and temporal resolution. An algorithm for storm identification and tracking using Tracking Radar Echoes by Correlation (TREC) technique (Rinehart, 1979) has been implemented. Storm cells are hence localized, characterized (i.e. maxima echo, storm area, Vertical Integrated Liquid) and tracked. Using this pattern recognition process radar derived storm cells are stored in arrays and they are compared by cross correlation with ones detected on previous step to determine storm path. Considering the overall path of the storm, it is then possible to nowcast next position of storms and their interaction with basins.

By integrating the new classification of alpine basins and the radar storm tracking method, PP7 has developed an innovative early warning system, called DEFENSE (DEbris Flows triggERed by storms - Nowcasting SystEm). The system is able to predict a dangerous torrential process that will involve roads and railways or other targets near to the alluvial fan area and/or to the main incised channel.

Recently Arpa Piemonte moved to a new approach, oriented to real time analysis and nowcasting derived products by full Geographic Information System (GIS) functionality based on Open Source platform and GFOSS tools. PostGIS allows for the native storage of geometries in the database and it allows for various GIS queries, including unions, area calculations and features within. Geometry objects can then be displayed by various GIS server and client applications, allowing the database to act as a backend GeoSpatial database for GIS servers.

Figure 4 shows storm centroids, simplified storm area and storm severity (area filled colour) and UTC time. Storm cells, whose centroids or precipitation interest or will interest in next 30 minutes basins, are identified and corresponding warnings are produced.

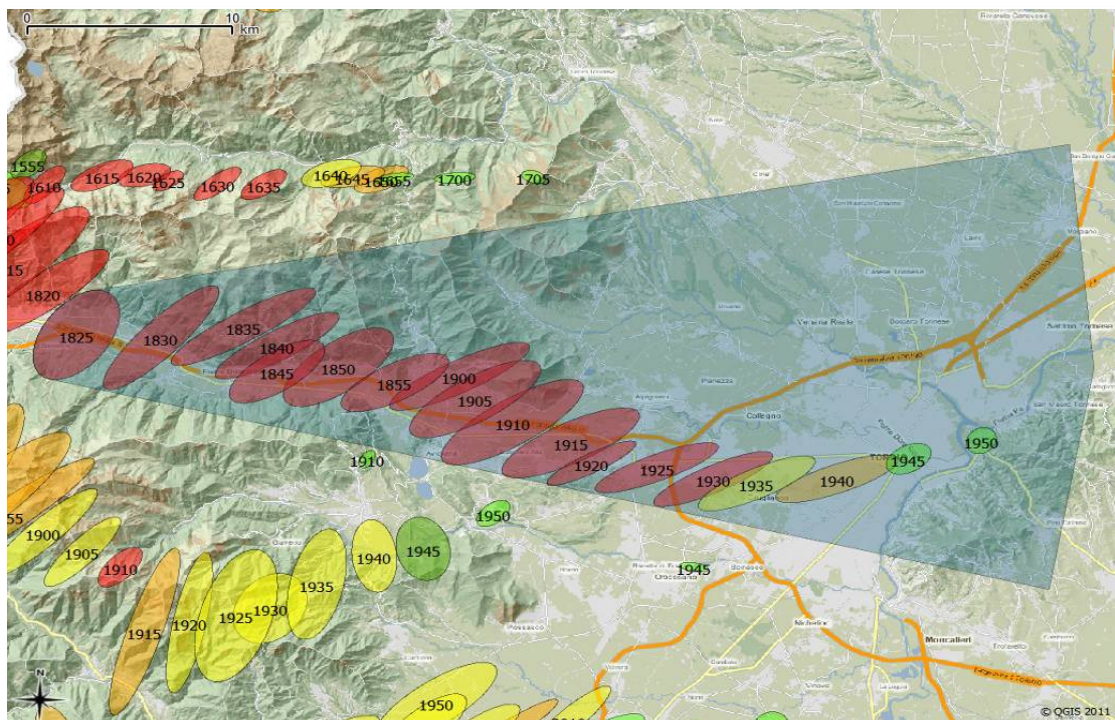


**Figure 4:** Example of storm tracking and nowcasting. Storm UTC time is showed, while colours identify storms' severity.

### 3 The Radar Storm Tracking

Rain gauge networks often miss localized and intensify precipitation (Duncan et al., 1993). Weather radars give a unique way to monitor rainfall over wide areas, with a high spatial detail and temporal resolution, provided that signal is above the minimum detectable signal.

The radar network is composed of two polarimetric C-band radars: the Bric della Croce radar, placed at 736 m asl on the top of the Torino hill and the Monte Settepani radar, located at 1,386 m asl on the Ligurian Apennines. Main technical characteristics of the C-band systems are listed in Table 1, while radars' position is displayed in Figure 5.

Features	Bric della Croce	Monte Settepani
Model	Meteor 400C	GPM250C
C-band frequency:	5,640 MHz	5,626 MHz
Antenna 3-B beam-width:	1°	1°
Antenna rotating speed:	6° to 36° sec <sup>-1</sup>	6° to 36° sec <sup>-1</sup>
Transmitter type	Magnetron	Klystron
Peak power:	250 kw	250 kw
Pulse duration:	1–2 μs	0.5–1.5–3 μs
Dual-polar:	H and V alternates (simultaneous since May 2008)	H and V alternates

**Table 1:** Main Arpa Piemonte radar characteristics.

The operational volume coverage pattern consists of a scan at 170 km range for the Bric della Croce radar (136 km for Settepani radar) with a set of 11 elevations (-0.1° to 28.5° for Bric, 0.3° to 28.5° for Settepani) and transmitting a short pulse (0.5 μs). Settepani also performs a secondary volume scan for qualitative monitoring at 250 km (3.0 μs pulse) with only three low elevations. The whole schedule is repeated every 5 minutes for both radars. Periodic six-monthly preventive maintenance is performed by the manufacturer on both radars. Electronic measurements during the maintenance tasks ensure that the radar constant is carefully checked and accurate within approximately 1 dB. In addition, an operational inter-calibration of the two radars is performed on a daily basis, when enough meteorological echoes are available in the overlapping region, by comparing the 3D volume scan intersecting bins. This check provides a useful way to detect eventual drift of one's radar calibration.

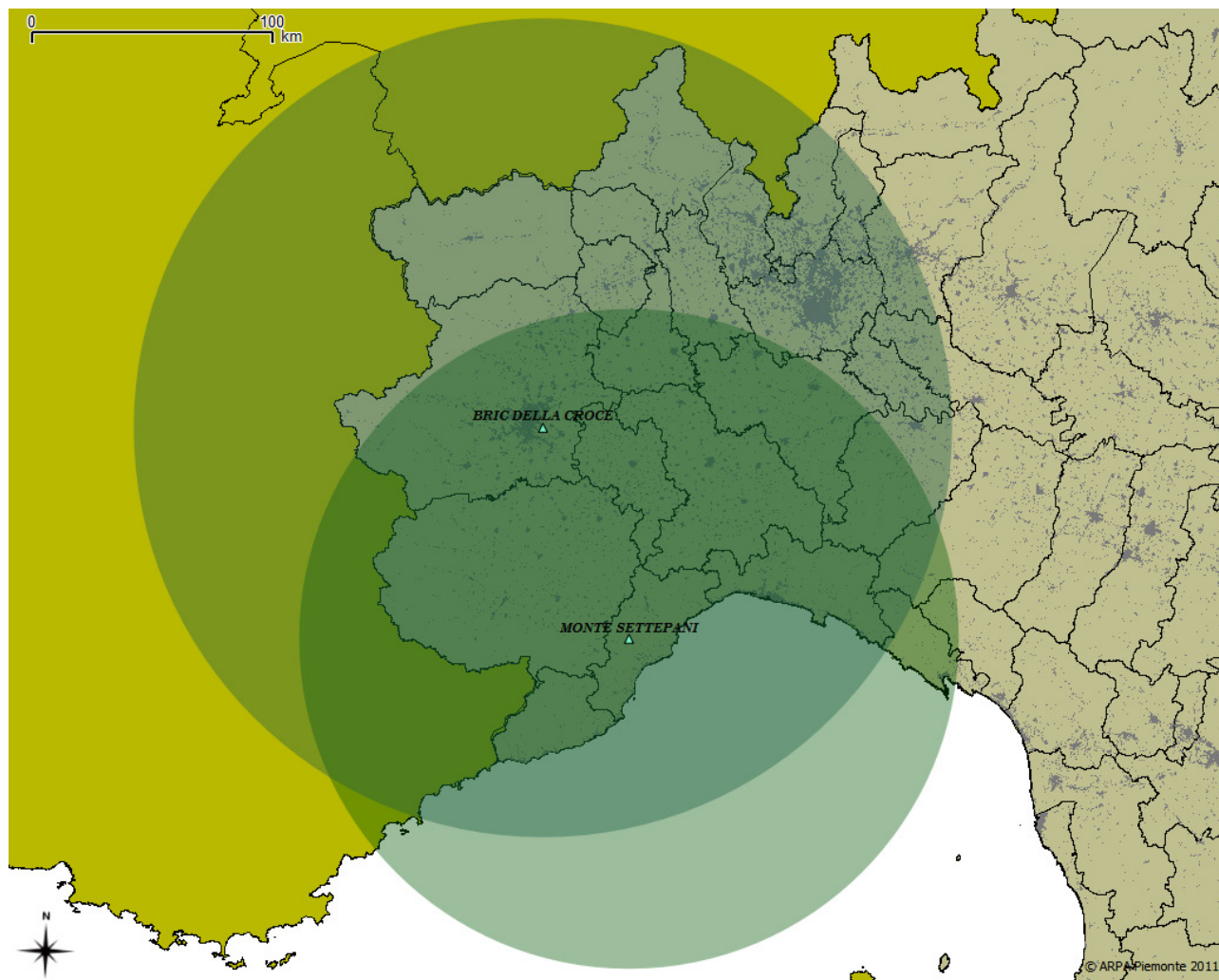


**Figure 5: Arpa Piemonte weather radar systems.**

Once the polar volume of reflectivity is flagged for clutter, a lowest level Cartesian map is derived for every radar. Initially a 2D polar map is computed, considering the first elevation free of orographic blocking at every (azimuth, range) location. The orographic blocking is estimated using the optical visibility calculated from a high resolution (50 m) digital elevation model. Subsequently the 2D polar map of lowest level reflectivity is transformed in Cartesian coordinates using a simple and fast nearest neighbor assignment. The geographical reference system for the Cartesian products is UTM ED50 (Universal Transverse Mercator, European Datum 1950). The coordinates of the radar maps are conventionally named utmX and utmY (distance along the x and y-directions in km within the fuse 32, covering North-Western Italy). The individual radar maps are then merged to form a radar composite for the North-Western Italy. Different criteria could be used in the merging process (mean, maximum, weighted mean, etc.). The operational procedure implements a weighted average for the merging, the weights being inversely proportional to the height of the radar beam above the ground (estimated from the same optical visibility maps used for the individual radar). The current Cartesian resolution of the radar composite is 800 m by 800 m. The reflectivity values are stored in the composite map, leaving to subsequent processing the conversion to rainfall intensity.

In order to identify convective cells, a storm identification and tracking algorithm has been employed. The storm tracking algorithm detects convective events with a maximum reflectivity larger than a given threshold and tracks them in space and time.

Convective cells are identified analyzing relative maximum values of surface rainfall estimated by the radar composite (Handwerker, 2002). To define a convective cell, all grid points on the composite map exceeding 40 dBZ are detected. Afterwards, all grid points exceeding 35 dBZ surrounding the

relative maximum already detected are associated to it: a minimum of 5 grid points on the radar domain (which is about 3 km<sup>2</sup> at the current radar resolution) must be identified, otherwise the cell is discarded. In this way, for each cell a centroid is defined. Storm cells area are simplified using confidence ellipses at 98% (Fox, 1997). Once active cells are localized, several meaningful storm parameters are computed and associated to the centroid: they can be derived by other composite products, as storm top, storm vertical-integrated liquid (VIL) (Doviak and Zrnic, 1984) or associated probability of hail, or derived by satellite data as cloud top and cloud temperature.

Moreover a Severity Storm Index (SSI), based on physical and statistical analysis of recorded storms, has been defined to synthesized the current dangerousness of cell. The approach for SSI definition is similar to rank algorithm used by MeteoSwiss (Hering et al., 2008). First of all a dimensionless storm severity, based on a subset of storm parameters, has been defined as:

$$\text{Storm Severity} = a1 * \text{VIL} + a2 * \text{Max echo} + a3 * \text{Echo top} \quad (1)$$

$$a1 = 1 / 10 \quad a2 = 1 / 20 \quad a3 = 1 / 200$$

where a1, a2, a3 are weighting factors for storm parameters. It's well-known that VIL is an hail-size indicator (Roger and Thompson, 1998; Amburn and Wolf, 1996), meanwhile updraft strength can be related with echo top height and peak reflectivity. Echo top gives information on vertical development of the cell (Cotton and Anthes, 1992). Max echo also provides an estimation of maximum instantaneous intensity of precipitation, associated to the storm.

Then quantiles from a climatological population of 2-year observations are derived.

$$\text{SSI} = \text{quantile} \{(\text{Storm Severity}), \text{prob}=[0.5,0.7,0.85,0.95,1.0]\} \quad (2)$$

The SSI ranges from 1 to 5 classes, corresponding to quantile calculated by (2). A sixth class has been added to take in account never recorded storm severity. Tracking is performed in two steps. At first all possible children of a certain parent reflectivity core are searched using the well-known COTREC technique (Rinehart and Garvey, 1978; Mecklenburg et al., 1999). In order to increase the reliability of the assignments, some constraints (derived from previous analysis) are applied to reduce the number of possible children: the maximum distance between parent and child reflectivity core is fixed at 8 km, the speed associated with the child core must be less than 3 times the parent one, and finally the new cell cannot reverse the direction of propagation with respect to the previous tracked ones (i.e. the maximum angle is fixed at 180°). Thereafter the assignments are reduced to more probable ones. In this way, all active convective cores within the observation area of the Arpa Piemonte radar systems are identified and tracked, providing storm information about the maximum reflectivity, the duration, the area covered by the convective cell, the travelled distance and other meaningful parameters.

## 4 The DEFENSE (DEbris Flows triggERed by storms - Nowcasting SystEm) model

Arpa Piemonte has developed since 2000 a WebGIS-based system to disseminate real time weather radar data and ground station data both for stakeholders and citizens. This application primarily focused on visualizing meteorological and hydrological data for decision support and situational awareness (Walawender, 2010). Recently Arpa Piemonte moved to a new approach, oriented to real-time analysis and nowcasting derived products, using full GIS functionality by the choice of Linux platform and GFOSS tools. The PostGIS extension allows for the native storage of geometries in the database and allows for various GIS queries to be made against the data, including unions, area calculations, and features within. Geometry features can then be displayed by various GIS (Geographic Information System) server and client applications, allowing the database to act as a backend GeoSpatial database for GIS servers. All storm parameters and paths are then stored in the same PostgreSQL/PostGIS database, where basins polygons are also stored. Storm cells with severity index above a fixed threshold ( $SSI > 3$ ), whose storm centroids or advective rainfall interest or will interest in next 30 minute a basin or basins group, are then localized and corresponding warnings are produced.

Every 5 minutes radar provides a raster image with corresponding levels of reflectivity. From measured dBZ could be estimated a value of precipitation.

As is not still possible to intersect directly raster image to basins polygons in PostGIS, it is necessary to accomplish some intermediate steps to get estimated rain on each defense basin.

So it is built a polygonal grid in PostGIS with same raster extent and spatial cell distance of 800 meters. The operation is performed “once and for all” through R, importing the radar's data as raster, transforming it in a SpatialPixelDataFrame (SPDF) object and importing it in PostgreSQL as a flat table and then expanded into polygon grid.

To each cell of the grid are associated the basins intersected following the relation “one cell-more basins”: this relationship is fixed if no changes occurs in the definition of the radar's raster production (extent and resolution).

The figure 6 show the process to determine the threshold exceed over the basins.

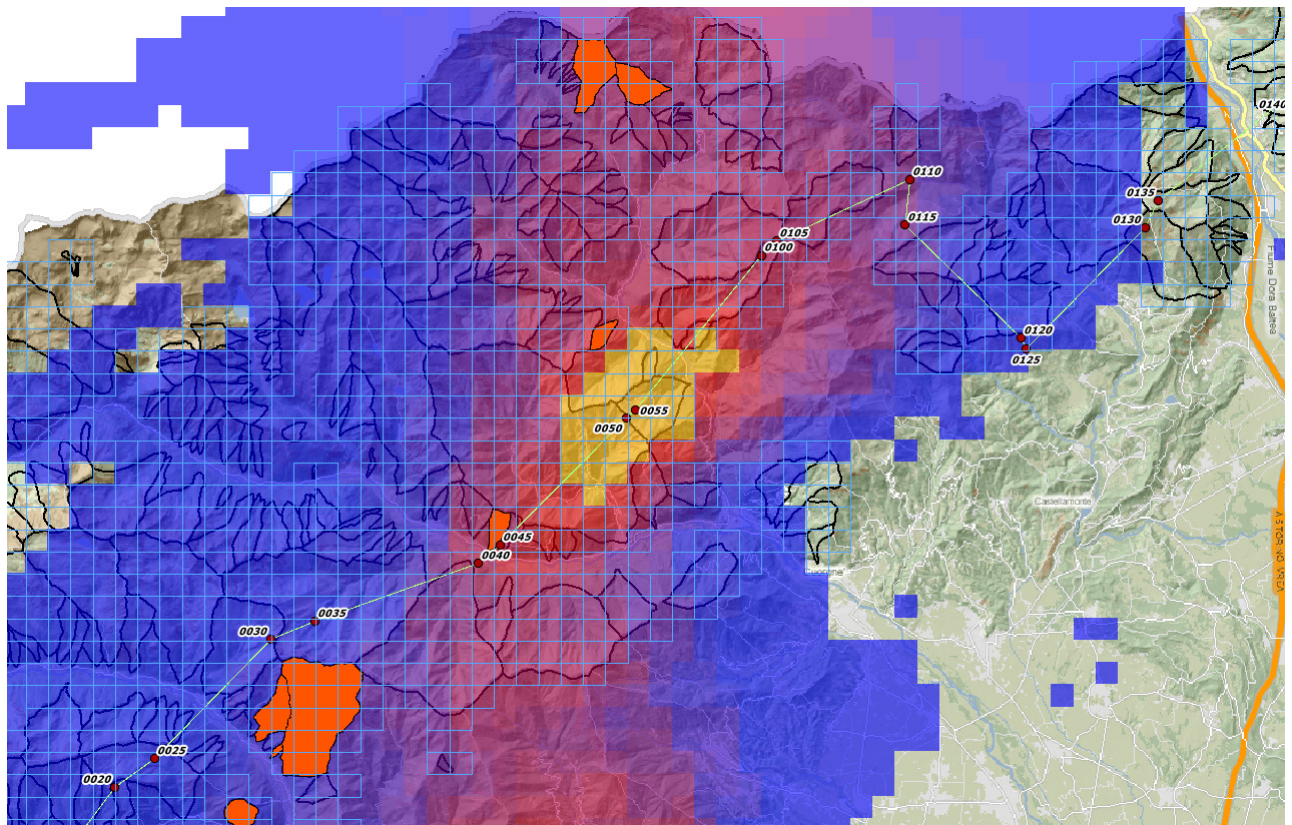


**Figure 6:** Grid associated to the basins intersected following the relation “one cell-more basins”.

The process going on at every new scanner of the radar is explicated as follows. The new radar's image is converted by R and send in PostgreSQL, then each cell of the new raster is joined to respective basins if any (based on the relationship mentioned before) and the precipitation is calculated for involved basins. If a threshold is exceeded, the basin is stored in a table and an alert is given.

The precipitation on the basins could be calculated in different ways:

- maximum value: among all the raster's cell intersecting the basin, the maximum is taking into account to describe the whole precipitation occurred;
- percentile: to avoid extreme value and anomalies, the 90th percentile of the various rain cells is assigned to the basin;
- weighted mean: as well as a simple mean of the values of precipitation occurred on the basins, it's possible to calculate a mean weighted on the percentage of the basin's area involved in the meteorological event.

To better understand the methodology to apply is fundamental to know that:

the precipitation calculated from radar measurements concern the high atmosphere and not the ground precipitation. So in presence of wind, for example, the rain cell defined could be relocated. Because of this, even cell intersecting small portion of a basin could be assigned and taken into consideration.

A debris flow could be triggered over any part of the basin (more probability on the upper section), so even a strong precipitation on a small portion could engender dramatical consequences.

The operational time of the procedures exposed above is about one minute. To have an overview of the whole meteorological situation in act, all the data are available on a real-time WebGIS user interface (Fig. 7) where storm, storm's paths, radar's images and basins on alert are displayed and refreshed every 5 minutes, together with data from the meteorological network. The WebGIS

interface allows also to query the raster data to know cell by cell the value of precipitation calculated, and to visualize the path of the storm and so to foresee the eventuality that other basins will be involved into meteorological event potentially debris flow triggering.

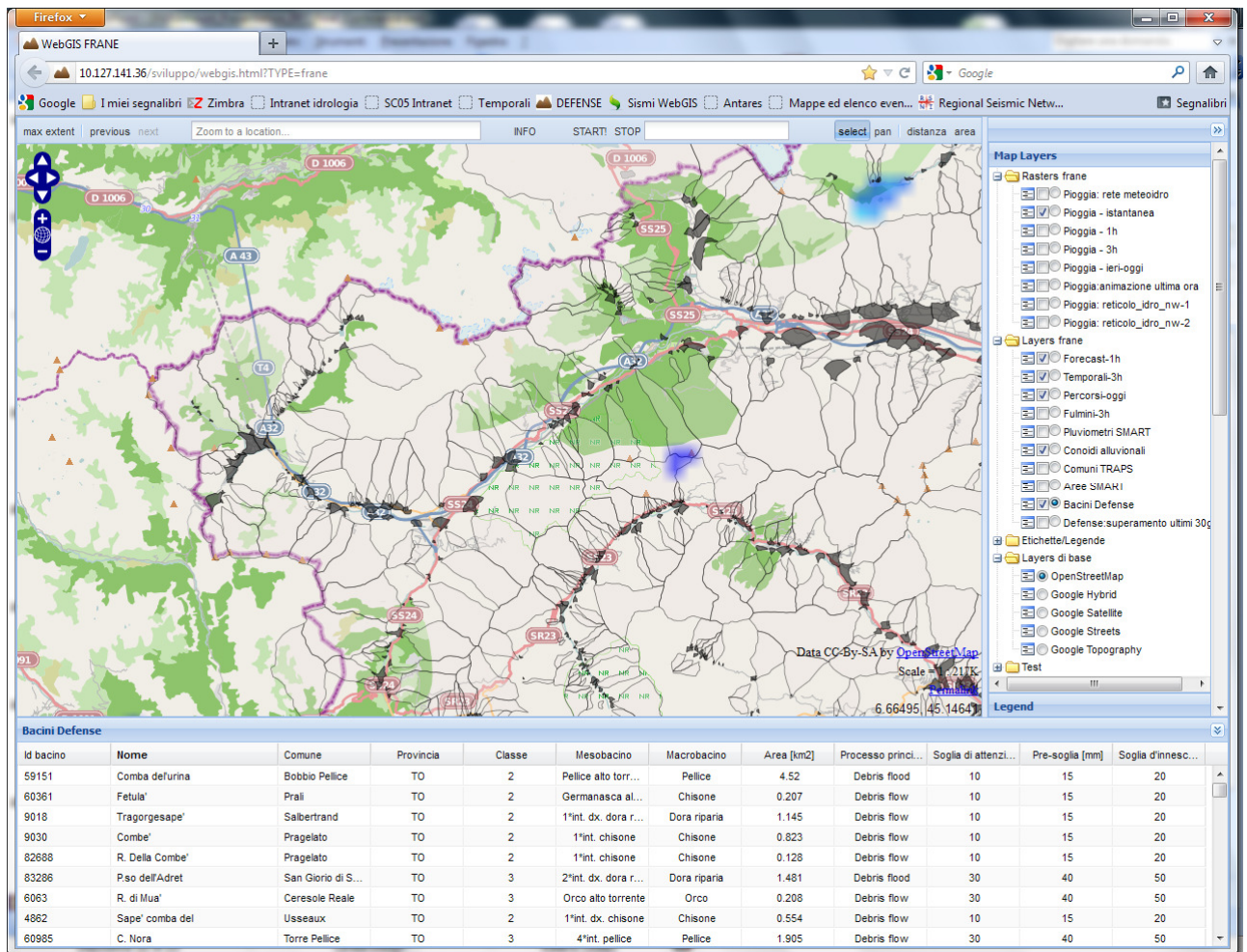


**Figure 7:** DEFENSE WebGIS interface: a zoom of Susa Valley. Basins are the not filled polygon outlined in black; alluvial fan are dark-gray polygons; highway in violet; railway is represented by dashed line; roads in pink; the borders Italy/France in fuchsia. The lower frame shows the basins parameters; the right frame collects all the layers of DEFENSE: raster radar maps ( with rainfall, hail and snowfall detection); storms (ellipsoids, centroids, observed and forecasted paths); lightnings distribution; basins and alluvial fans; geographical maps (including dem); structures and infrastructures.

## 5 DEFENSE operational results in Susa Valley

On September 3<sup>rd</sup>, 2011 an atmospheric low pressure area (Fig. 8), moving from the Balearic Islands towards the Sea of Sardinia, causes a wet southern flow and atmospheric instability in the afternoon responsible of widespread and strong storm activity over north-western Alpine foothills. A storm event hit Susa Valley causing mud-debris floods/mud-debris flows in three basins of Susa Valley (T. Claretto, T. Gioglio and T. Mardarello - Val Cenischia, Torino) at 13:30-14:00 UTC. Several damages were reported, including severe damages to the only access route to the valley (Fig. 9).

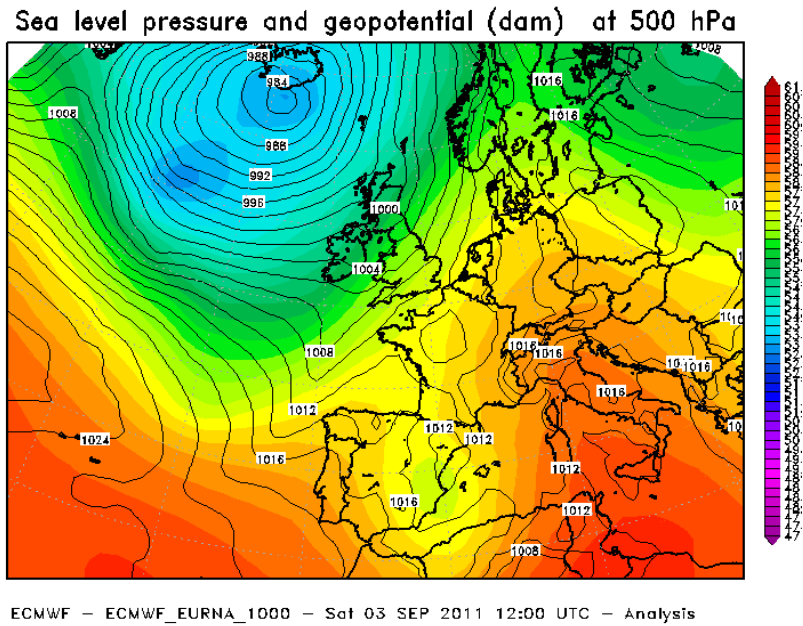


**Figure 8:** Map of sea level pressure and geopotential at 500 hPa on September 3rd 2011, 12:00 UTC.



**Figure 9:** Only access route to the Cenischia valley, damaged by mud-debris flow (T. Gioglio).

The basins of T. Gioglio, T. Claretto and T. Mardarello can be ascribed to the basins of Class 2 in which the basin's bedrock is mainly formed by finely-foliated metamorphic rocks rich in phyllosilicates (such as phyllitic schists and calc-schists in this case) (Fig. 10). The high production of

clay-like minerals in loose material determines a viscoplastic rheology of debris flow/debris flood phenomena.

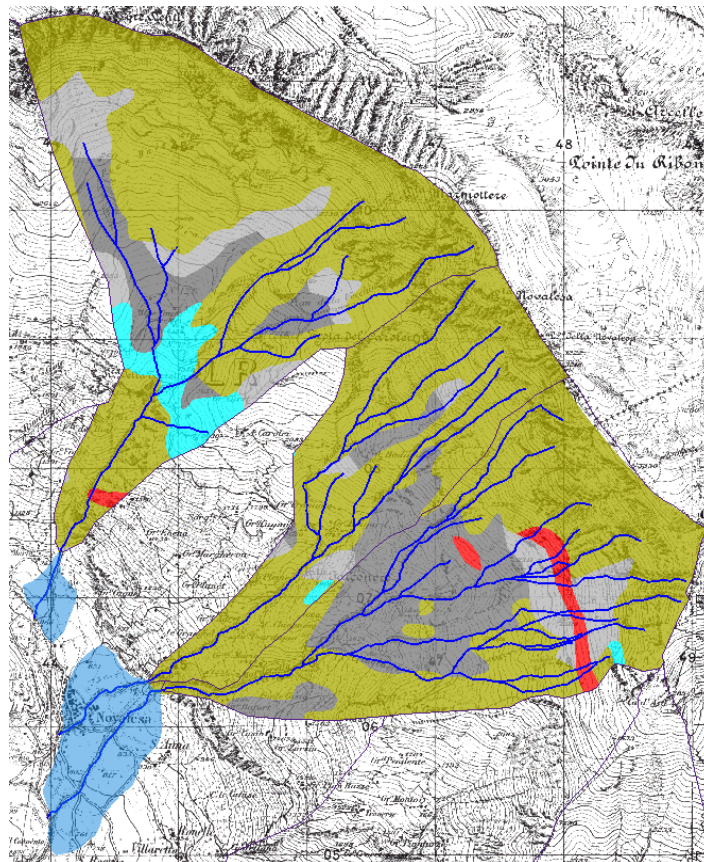


**Figure 10:** Lithological settings of (from north to south) T. Gioglio, T. Claretto and T. Marderello catchments : calc-schists and phyllades in ocher; limestones and dolostones in light-blue; anphybolites and prasinites in red; talus deposits in light-gray; glacial deposits in dark-gray.

On the basis of the main morphometric characteristics of the catchment it is possible to identify the most likely type of torrential process characterized by different hazard degree that may occur in alluvial fan area (Wilford et al., 2004):

Table BB shows the morphometric data of the main basins examined: the basin area ( $Ab_{plan}$  in  $km^2$ ), the effective basin surface area ( $Ab_{eff}$  in  $km^2$ ), the effective longitudinal extension of the basin (Elong in km), the energy can be discerned (H in km) given by the difference between the maximum elevation value and the minimum one in basin, the index of Melton (Me) and finally the alluvial fan area/basin area (Af/Ab) ratio.

Basin	$Ab_{plan}$	$Ab_{eff}$	Elong	H	Me	Af/Ab
T. Gioglio	7.22	10.24	4.06	2.48	0.92	0.10
T. Claretto	3.40	5.15	4.14	2.42	1.31	0.41
T. Marderello	5.39	6.87	4.40	2.63	1.13	3.35

**Table 2:** Main morphometric data of the studied basins.

The most likely expected process for these three basins is a debris flood, rich in fine fraction.

By weather radar observations, storms responsible for DFds/DFws triggering were identified as individual cells, following their evolution with satisfactory accuracy (Fig. 11). As showed in Figure 11, some storm cells followed a south-to-north path coincident with the axis of the Cenischia Valley (Susa Valley), getting close to the basins affected by mud-debris floods/ mud-debris flows.

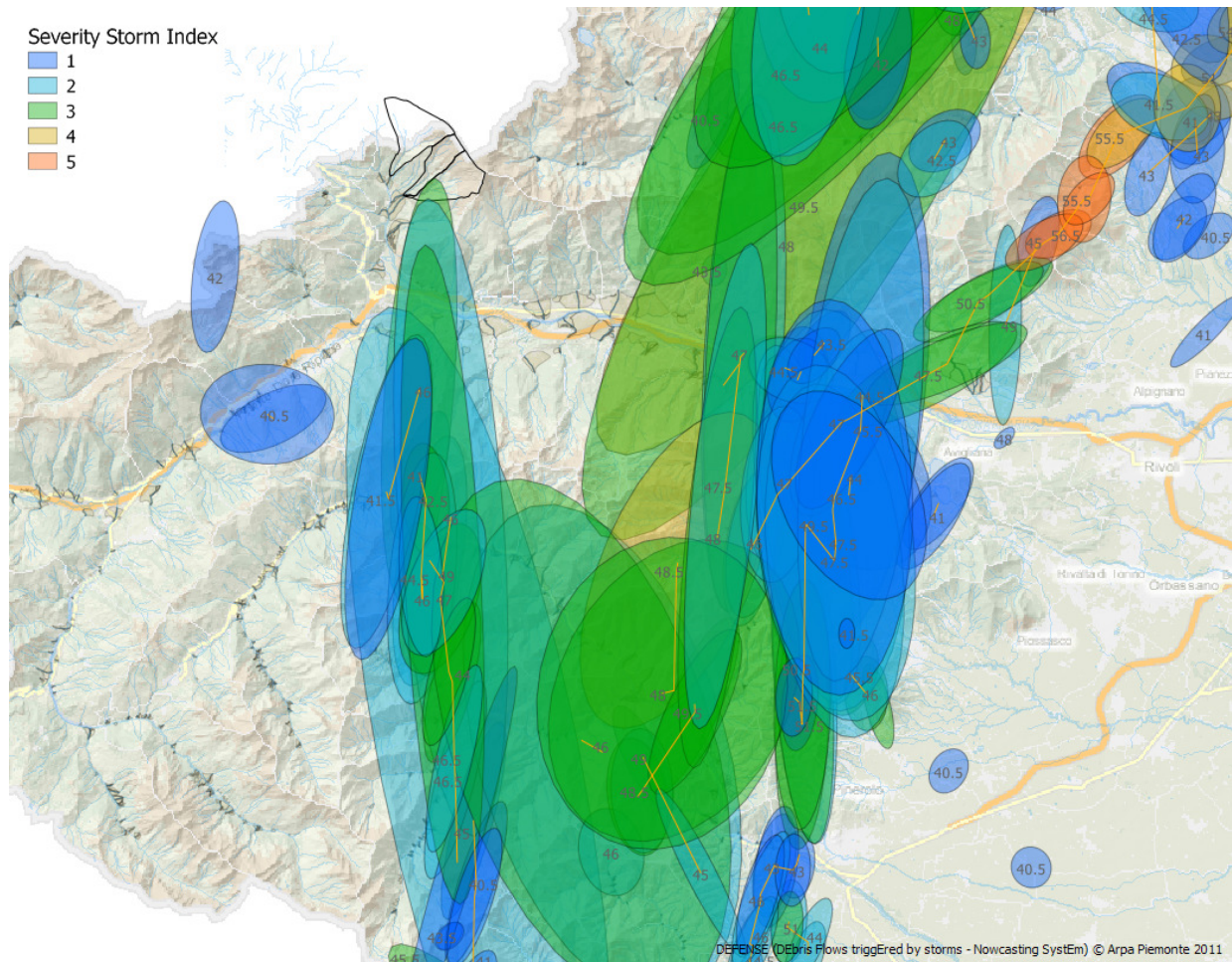


**Figure 11:** Storm cells paths. The numbers on cells centroids are the reflectivity values (dBZ). Involved basins bordered in black.

By weather radar it was possible to estimate instantaneous precipitation fields during the event. The rainfall amount estimated by the radar observations are obtained by the conversion of the reflectivity values (dBZ) into rain values (mm) using Marshal & Palmer relationship with  $A = 300$  and  $B = 1.5$ . Precipitation fields at 13:40 UTC over the hit area is represented in Figure 12, showing that the most intense storm-shower (about 45 dBZ corresponding to 22 mm) affected the three basins mostly in head areas.

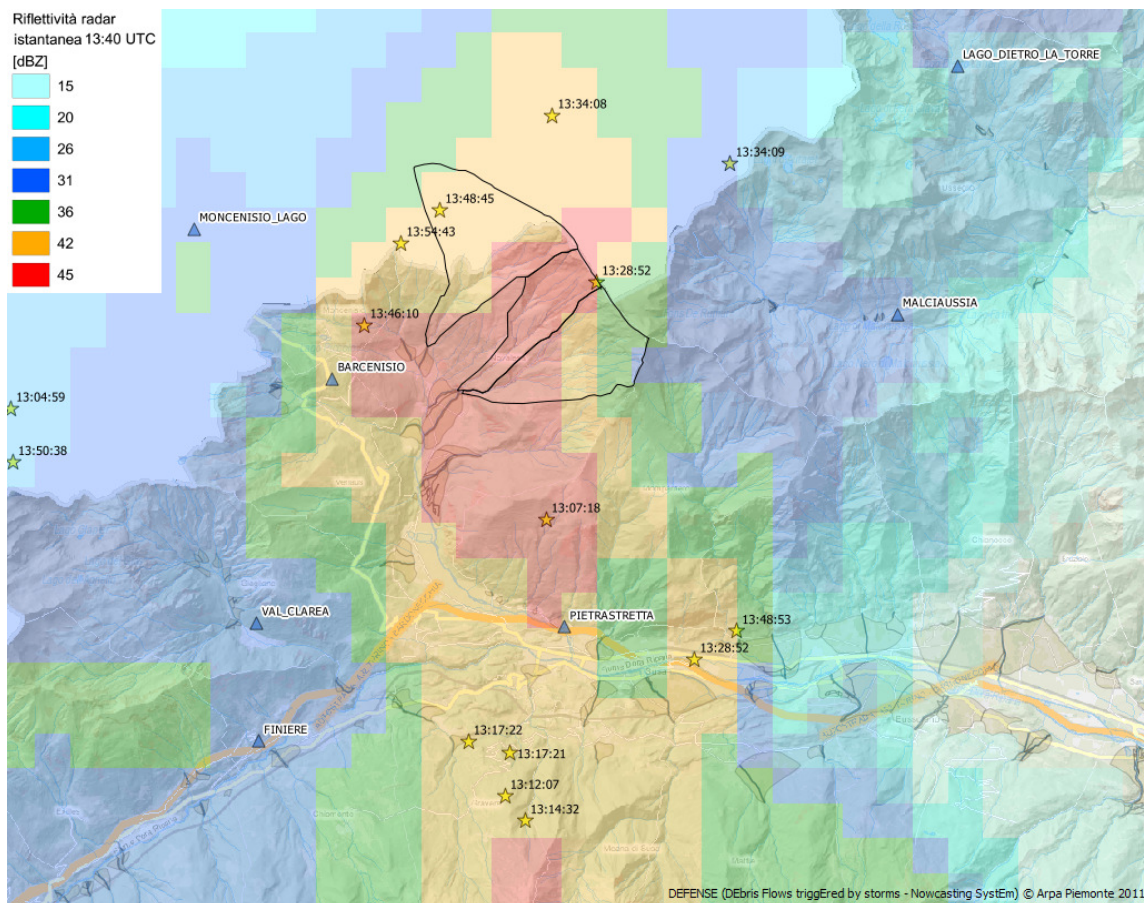


**Figure 12:** Rainfall intensity distribution by radar during the critical storm event for the initiation of mud-debris floods/mud-debris flows. Lightning activity is represented by star symbols; rain gauges as blue triangles.

The verifications of radar estimated rainfall is obtained by the comparison with the rainfall recorded by rain gauges closest to the basins. The comparison for the event was made by taking into account the measurements by the Barcenisio rain gauge located about 5 km far from interested basins.

The rainfall amount over three basins was reconstructed using the spatial distribution of precipitation derived from radar measurements and adjusted according to Barcenisio rain gauge (Tab. 3). The rain, that affected the three basins, are characterized by intensity and cumulative values higher than recorded by the Barcenisio rain gauge.

Time interval	Maximum rainfall intensity [mm]	Occurrence interval of maximum rainfall intensity (UTC)
10 min	8.2	13:40-13:50
30 min	18.6	13:30-14:00
1 h	24	13:10-14:10
2 h	31.2	13:00-15:00

**Table 3:** Rainfall values recorded by Barcenisio rain gauge.

In particular, the average basins cumulative rainfall between 13:00 and 15:00 UTC was about 43 mm in T. Claretto and T. Mardarello, and approximately 33 mm in T. Gioglio (Fig. 13).

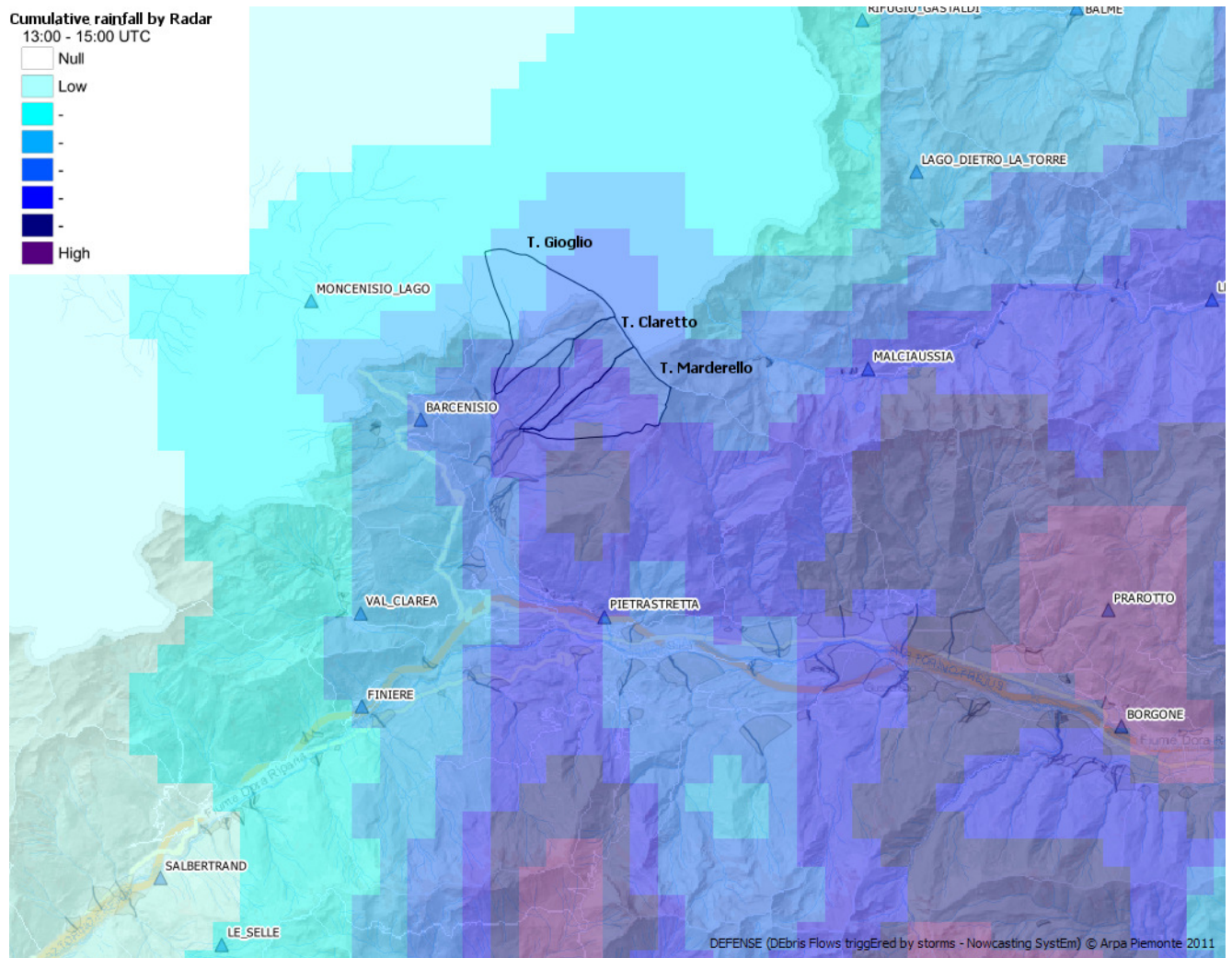


**Figure 13:** Radar map of cumulative rainfall from 13:00 to 15:00 UTC. Rain gauges as blue triangles.

In conclusion, the mud-debris floods/mud-debris flows were triggered only in those basins affected by the strongest storm shower responsible for the excess of Class 2 basins triggering-thresholds ( $\geq 20$  mm/h).

## 6 Concluding remarks

A real-time torrential processes forecast system has been here presented. The system is based both on proper basins classification and on storm identification and tracking algorithm using operational polarimetric C-band radar operated by Arpa Piemonte. System architecture is implemented by OpenGIS packages. Storm cells centroids and parameters are stored in PostGRES/PostGIS database and geographical operation are there performed to derive critical conditions. Data, indicating critical basins interested by severe storms, are produced every 5 minutes and published on WebGIS server.

Whole system (basins classification and radar monitoring and nowcasting) can be easily applied over the Alps and generally in mountainous areas. This innovative system can be operationally implemented for WebGIS based early warning issues to roads, railways and infrastructures stakeholders (Civil Protection, Road managers, etc). Moreover mobile apps/web apps can learn citizens of current alerts and what to do in response to the situation. These alerts can be filtered through various options which include; location (by choice or by GPS), severity and type. Users can then decide interval to use when refreshing alerts. Once set up, you can then navigate through the specified alerts. Detailed information can be also available like affected locations, effective date/time and occurrence probability.

## Acknowledgements

PP7 Project Responsible: Dr. Anna Maria Gaffodio - Head of the Department of Forecasting Systems, Arpa Piemonte (Regional Agency for Environmental Protection of Piemonte), Turin, Italy.

PP7 Authors: Dr. Davide Tiranti and Dr. Roberto Cremonini - Hydrology and Natural Hazards, Department of Forecasting Systems, Arpa Piemonte (Regional Agency for Environmental Protection of Piemonte), Turin, Italy.

With contributions from Dr. Armando Riccardo Gaeta - Hydrology and Natural Hazards, Department of Forecasting Systems, Arpa Piemonte (Regional Agency for Environmental Protection of Piemonte), Turin, Italy, and, Dr. Federica Marco and Rocco Pispico - Department of Geology and Geohazards, Arpa Piemonte (Regional Agency for Environmental Protection of Piemonte), Turin, Italy.

## References

- Amburn S. and Wolf P. (1996) VIL Density as a Hail Indicator. 18th Conference on Severe Local Storms. San Francisco, CA, Amer. Meteor. Soc., 581-585.
- Cotton W.R. and Anthes R.A. (1992) Storm and Cloud Dynamics (International Geophysics Series), Academic Press, San Diego, USA.
- Doviak R.J., Zrnic D.S. (1984) Doppler radar and weather observations. New York, Academic Press, Edition 1993; pp. 458.
- Duncan M.R., Austin B., Fabry F., Austin G.L. (1993) The effect of gauge sampling density on the accuracy of streamflow prediction for rural catchments. Journal of Hydrology, 142, Issues 1-4, Pages 445-476, ISSN 0022-1694.
- Fox, J. (1997) Applied Regression, Linear Models, and Related Methods. CA: Sage Publications, 1997, ISBN 0-8039-4540-X, 597 pp.
- Handwerker J. (2002) Cell tracking with TRACE3D: a new algorithm. Atmospheric Research, 61, 15 – 34.
- Hering A. M., German U., Galli G., Boscacci M, Sényesi S. (2008) Operational nowcasting of thunderstorms in the Alps during MAP D-PHASE. In: Proceedings of the 5th European Conference on Radar Meteorology (ERAD 2008), June 30 - July 4, Helsinki, Finland.

Mecklenburg S., Schmid W., Joss J. Cortec (1999) A simple and reliable method for nowcasting complex radar pattern over complex orography. Final Seminar of COST-75: An Advanced Weather Radar Systems, 61, 441–450.

Rinehart R.E. and Garvey E.T. (1978) Three-dimensional storm motion detection by conventional meteorological radar. *Nature*, 273, 287–189.

Roger E., Thompson R.L. (1998) Nationwide comparisons of hail size with wsr-88d vertically integrated liquid water and derived thermodynamic sounding data. *Wea. Forecasting*, 13, 277–285.

Tiranti D. (2008) The sediment gravity flows triggering mechanisms, evolution and sedimentary processes in Western Italian Alps. Ph.D. Dissertation - Department of Earth Sciences, University of Torino (Italy) and the Cambridge Quaternary, Department of Geography, University of Cambridge (United Kingdom); pp. 100.

Tiranti D., Bonetto S., Mandrone G. (2008) Quantitative basin characterization to refine debris-flow triggering criteria and processes: an example from the Italian Western Alps. *Landslides*, 5(1): 45-57.

Walawender B.P., Davis M.W. (2010) Development of web-based gis applications for decision support and situational awareness. In: 26th Conference on Interactive Information and Processing Systems (IIPS) for Meteorology, Oceanography, and Hydrology.

Wilford D.J., Sakals M.E., Innes J.L., Sidle R.C. and Bergerud W.A. (2004) Recognition of debris flow, debris flood and flood hazard through watershed morphometrics. *Landslides* 1(1): 61-66.

## Table of figures

Figure 1 : The classified basins of Susa Valley: G1 basins in light blue; G2 basins in green; G3 basins in dark red. ....	1
Figure 2: The graph represents the basins of Susa Valley subdivided by lithological group and statistical occurrence of process types in each group. G1 in light-blue, G2 in green, G3 in red; FF = flash flood; DFd = debris flood; DFw = debris flow. ....	2
Figure 3: Main expected phenomena in Susa Valley’s basins. Flash Flood in light blue; Debris Flood in orange; Debris Flow in red. ....	3
Figure 4: Example of storm tracking and nowcasting. Storm UTC time is showed, while colours identify storms’ severity.....	4
Table 1: Main Arpa Piemonte radar characteristics.....	5
Figure 5: Arpa Piemonte weather radar systems.....	6
Figure 6: Grid associated to the basins intersected following the relation “one cell-more basins” .....	9
Figure 7: DEFENSE WebGIS interface: a zoom of Susa Valley. Basins are the not filled polygon outlined in black; alluvial fan are dark-gray polygons; highway in violet; railway is represented by dashed line; roads in pink; the borders Italy/France in fuchsia. The lower frame shows the basins parameters; the right frame collects all the layers of DEFENSE: raster radar maps ( with rainfall, hail and snowfall detection); storms (ellipsoids, centroids, observed and forecasted paths); lightnings distribution; basins and alluvial fans; geographical maps (including dem); structures and infrastructures. ....	10
Figure 8: Map of sea level pressure and geopotential at 500 hPa on September 3rd 2011, 12:00 UTC. ....	11
Figure 9: Only access route to the Cenischia valley, damaged by mud-debris flow (T. Gioglio).....	11
Figure 10: Lithological settings of (from north to south) T. Gioglio, T. Claretto and T. Marderello catchments : calc-schists and phyllades in ocher; limestones and dolostones in light-blue; anphybolites and prasinites in red; talus deposits in light-gray; glacial deposits in dark-gray.....	12

Table 2: Main morphometric data of the studied basins.....	12
Figure 11: Storm cells paths. The numbers on cells centroids are the reflectivity values (dBZ). Involved basins bordered in black. ....	13
Figure 12: Rainfall intensity distribution by radar during the critical storm event for the initiation of mud-debris floods/mud-debris flows. Lightning activity is represented by star symbols; rain gauges as blue triangles.....	14
Table 3: Rainfall values recorded by Barcenisio rain gauge. ....	14
Figure 13: Radar map of cumulative rainfall from 13:00 to 15:00 UTC. Rain gauges as blue triangles.	15